Structure−property relations of 55 nm particle-toughened epoxy

Quyen-Huyen Le [a], Hsu-Chiang Kuan [b], Jia-Bin Dai [a], Izzuddin Zaman [a], Lee Luong [a], Jun Ma [a,*]

[a] School of Advanced Manufacturing and Mechanical Engineering, University of South Australia, Mawson Lakes, South Australia 5095, Australia
[b] Department of Energy Application Engineering, Far East University, Tainan County 744, Taiwan

ARTICLE INFO

ABSTRACT

55-nm rubber particles significantly toughened two epoxy systems without loss of Young's modulus, tensile strength and glass transition temperature. Transmission Electron Microscopy (TEM) showed that the nanoparticles are uniformly dispersed in matrix and have blurred interface with epoxy. 5 wt% rubber nanoparticles increased the critical strain energy release rate (G_{1c}) of Jeffamine D230 (J230)-cured epoxy from 175 J/m^2 to 1710 J/m^2, while the 10 wt% increased G_{1c} of diaminodiphenyl sulfone (DDS)-cured epoxy from 73 J/m^2 to 696 J/m^2. This is explained by comparing the surface–surface interparticle distance and total particle surface of nanocomposites with those of composites. The higher the matrix stiffness, the more nanoparticles needed for toughening. Although the 10 wt% J230-cured nanocomposite showed a 50% larger size of stress-whitened zone than the 5 wt% J230-cured nanocomposite, the 5 wt% nanocomposite showed a higher toughness. These nanoparticles were found to pose barriers to the vibration of crosslinked matrix molecules, leading to higher glass transition temperatures. While the matrix shear banding caused by nanoparticle expansion and growth is the major toughening mechanism for the J230-cured nanocomposites, the matrix plastic void growth and deformation are most probably the major mechanisms for the DDS-cured system. Under tensile loading, the nanoparticles in the DDS-cured epoxy created fibrils of 100−200 nm in diameter and 3−5 μm in length. TEM analysis in front of a subcritically propagated crack tip showed a number of voids of 30−500 nm in diameter in the vicinity of the crack, implying that rubber nanoparticles expanded, grew and deformed under loading. Unlike conventional epoxy/rubber composites in which all of the rubber particles in the crack front cavitated under loading, only a portion of the nanoparticles in this study expanded to create voids. Huang and Kinloch's model developed from composites was found not fit well into these nanocomposites.

© 2010 Elsevier Ltd. All rights reserved.

1. Introduction

For the past decades, extensive studies have been conducted on toughening epoxy resins by rubbers, thermoplastics, inorganic particles, etc. Rubber and thermoplastic toughening methods require a substantial amount of toughener, e.g. 15−20 wt%, which causes loss of other desirable properties. For example, compounding 15 wt% rubber with DGEBA improved the fracture toughness from 0.75 to 1.48 MPa m$^{1/2}$ but caused 27% modulus loss [1].

Nanomaterials are of great potential for novel tougheners, and thus attracted intensive interest in both academia and industry. Numerous studies [2−9] compounded silicate layers with epoxy resins, but the toughening effect is not ideal due to the weak interface between the layers and the resins. Recently, silica nanoparticles have been adopted to stiffen and toughen epoxy resins [10−16]. It

shows that 20 wt% silica nanoparticle fraction provided 40% improvement in Young's modulus and simultaneously improved the toughness from 0.73 to 1.68 MPa m$^{1/2}$ [14]. There are a number of explanations for toughening mechanisms: the breakage of chemical bonds [10], nanoparticle debonding followed by plastic void growth [13], shear banding [15] and the local plastic deformation [16]. Our research shows that toughening was contributed by matrix dilatation which was induced by nanovoid formation and growth [14]; no interface debonding of nanoparticles was found, as opposed to their peer micron-sized particles [17−19].

Rubbers have remained the most popular tougheners due to their significant toughening effect. In conventional epoxy/rubber composites, liquid rubber forms 1−10 μm particles during curing, and the principal toughening mechanism is the internal cavitation of rubber particles in the slow growth zone followed by massive matrix shear yielding [20]. When the particle size reduces to below 100 nm, the toughening mechanism is reported as rubber particle cavitation followed by the shear banding of epoxy matrix [21]. We *in situ* formed 2−3 nm rubber particles for toughening epoxy [22].
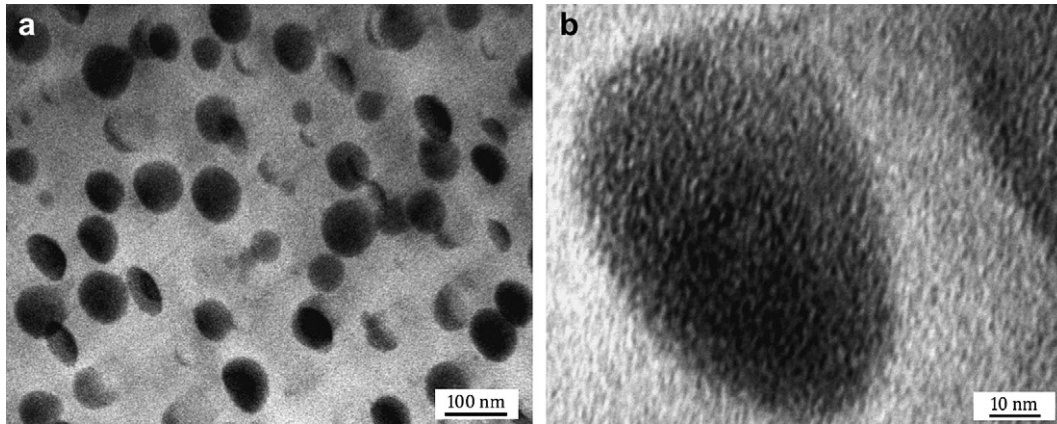
Fig. 1. TEM micrographs of the 10 wt% J230-cured nanocomposite.

At similar tougheners' contents, rubber nanoparticles toughened as effectively as conventional rubber, but caused much less Young's modulus deterioration. Since neither particle cavitation nor deformation was observed, the toughening mechanism was attributed to the stress relaxation of the matrix, which led to larger plastic work absorbed at the crack tip. However, it is not clear (i) whether the rubber particles ranging between 100 nm and 3 nm can produce a more significant toughening improvement than previous effort [23,24] with no loss of other important properties, like stiffness and yield strength, and (ii) are there other toughening mechanisms apart from the reported cavitation and matrix shear yielding?

In this study, we will employ commercially available 55-nm rubber particles to toughen two epoxy systems. The structure–property relations of polymer nanocomposites will be illustrated by investigating the morphology, mechanical properties, fracture toughness, thermal mechanical behaviour, fracture surface and toughening mechanisms of these systems, with special attention on the role of nanoparticles on crack propagation when fracture occurs.

2. Experimental section

2.1. Materials

Epoxy resin Diglycidyl Ether of Bisphenol A (DGEBA, Araldite-F) with an epoxide equivalent weight 182–196 g/equiv was supplied by Ciba-Geigy, Australia. The spherical rubber nanoparticles (Kane ACE MX-120) were supplied as a colloidal sol (25 wt%, EEW 243 g/equiv) in epoxy by Kaneka, Japan. Hardener Jeffamine D230 (denoted J230) was kindly provided by Huntsman (Singapore); hardener 4,4′-Diaminodiphenyl sulfone (denoted DDS) was purchased from Chriskev Company, Inc., USA.

DGEBA was mechanically mixed with given amounts of the master batch of epoxy/nanorubber at 100 °C for 60 min to produce a series of nanocomposites with 0–10 wt% rubber contents. Then the mixtures were blended with the two hardeners by the following
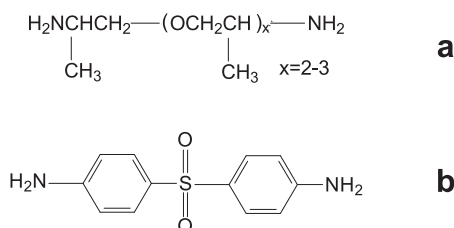
procedures, respectively. (1) When the mixtures were cooled down to 50 °C, stoichiometric amounts of the curing agent J230, calculated from the DGEBA and the master batch, were respectively blended with the mixtures for 5 min, followed by degassing. Finally it was poured into release agent-coated rubber moulds and cured at 80 °C for 3 h, followed by 12 h at 120 °C. Samples were taken out when the oven cooled to 50 °C after curing. Or (2) the mixing temperature increased to 130 °C. Calculated from the DGEBA and the master
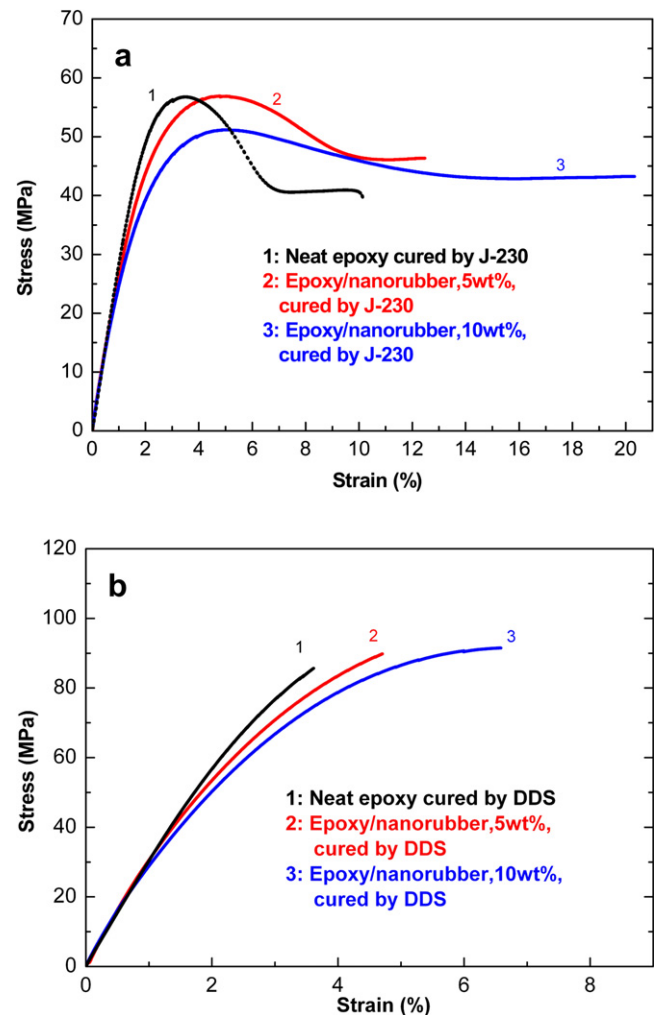

Fig. 2. Hardeners used in this study: (a) J230 and (b) DDS.

Fig. 3. Stress–strain curves of the two epoxy systems cured (a) by J230 and (b) by DDS.

Table 1
Mechanical properties and toughness of neat epoxy and nanocomposites cured by J230.

Materials	Young's modulus, GPa	Tensile strength, MPa	Plane-strain fracture toughness, K_{1c}, MPa m$^{1/2}$	Critical strain energy release rate G_{1c}, kJ/m^2
Neat Epoxy, cured by J230	2.75 ± 0.10	57.1 ± 0.5	0.73 ± 0.07	0.175 ± 0.037
Nanocomposite, 2.5 wt%, cured by J230	2.77 ± 0.09	57.5 ± 0.6	1.96 ± 0.06	1.232 ± 0.080
Nanocomposite, 5 wt%, cured by J230	2.74 ± 0.12	57.0 ± 0.3	2.29 ± 0.06	1.710 ± 0.090
Nanocomposite, 10 wt%, cured by J230	2.65 ± 0.17	52.2 ± 1.0	1.82 ± 0.05	1.116 ± 0.057

batch, stoichiometric amounts of DDS were respectively blended with the mixtures for 10 min, followed by curing at 130 °C for 17 h.

2.2. Morphology

Diamond knife and Leica Ultracut S microtome were used for ultra-thin sections of ∼50 nm in thickness; sections for microstructure were made at −120 °C, while sections for fracture mechanism were obtained at room temperature, as microtoming at room temperature minimizes damages to the sections. Sections were collected on 200-mesh copper grids, stained with 5 wt% osmium tetroxide for 12 h and examined using a Philips CM200 Transmission Electron Microscope (TEM) at an accelerating voltage of 200 kV.

Scanning electron microscopy (SEM) was used to examine the fracture surfaces of tensile samples and compact tension (CT) specimens, which were coated with a thin layer of gold and observed using a Philips XL30 FEGSEM at an accelerating voltage 10 kV. Particle sizes were analyzed using an image analysis software analySIS®.

2.3. Mechanical property

Tensile dumb-bell samples with a gauge length of 50 mm were made using a silicone rubber mold and both sides were polished by emery paper until all visible marks disappeared. Then the samples were post-cured at 120 °C for 60 min to diminish the defects caused by polish. Tensile testing was performed at a strain rate of 0.5 mm/min at room temperature using an Instron 5567 tensile machine. An Instron extensometer 2630-100 was used to collect accurate displacement data to measure the modulus; Young's moduli were calculated using 0.005−0.2% strain.

2.4. Fracture toughness

The CT samples were cured in the mold and then both sides were polished by emery paper until all visible marks disappeared. We introduced an instantly propagated crack to each sample, which is critical to toughness testing, by a razor blade tapping method [25]. Six specimens were tested for each set of data with a crosshead speed of 0.5 mm/min. The K_{1c} and G_{1c} values of CT specimens were calculated and verified according to ISO13586.

2.5. Dynamic mechanical analysis (DMA)

Dynamic mechanical spectra were obtained at a frequency of 1 Hz on a DMA 2980 Dynamic Mechanical Analyzer (TA Instruments, Inc., USA). A single cantilever clamp with a supporting span of

20.00 mm was used. The rectangular specimen with a thickness of 4 mm and width of 12 mm was tightened on the clamp using a torque of 1 Nm. Data were recorded at a sampling rate of 2 s/point.

2.6. Toughening mechanisms

2.6.1. Optical microscopy (OM) analysis

A thin section perpendicular to the fracture surface was prepared for OM. The fractured CT sample was potted in a room-temperature curing epoxy, and then a 40-μm thick section was produced by polishing the two sides perpendicular to the fracture surface. The section was viewed by a Nikon microscope using crossed-polarized light. A quarter wave plate was used to enhance the contrast of the birefringent regions.

To identify the toughening mechanisms of high modulus thermoset, we developed a tailor-loaded CT method [14], which provides quantitative deformation of nanoparticles in front of a sharp crack tip prior to propagation. A critical load for a sharp crack is the minimum load which propagates the crack. Since the 55-nm rubber particles significantly toughened epoxy as shown in the following text, 50% of the critical load was defined as the subcritical load which applied to a sharp crack. A sharp crack loaded under a subcritical load is called a subcritical crack.

3. Results and discussion

3.1. Microstructure

Fig. 1 shows typical TEM micrographs of the J230-cured nanocomposite with 10 wt% nanoparticles—the highest rubber fraction in this study. As described in Section 2, the sections were stained by osmium tetroxide, during which the rubber particles absorbed more osmium tetroxide than the matrix did and thus the particles should appear dark in the micrographs. At a low magnification in Fig. 1a, the rubber nanoparticles are indeed dark and uniformly dispersed in the epoxy matrix with a narrow size distribution; blurred interface is obvious at a high magnification in Fig. 1b. When ethylene−propylene diene monomer rubber was mixed with nylon, a distinct interface was observed; in contrast, a blurred interface was found when chlorinated polyethylene was reactively mixed with nylon [see Fig. 3 of Ref. [26]]. Thus, it is reasonable to assume a strong interface between epoxy matrix and rubber nanoparticles. The interface between epoxy and its dispersion particles has been found critical in determining the *in situ* formed particle size and the toughening effect [27,28]. A particle size of 55.4 ± 19.0 nm was obtained through image analysis conducted on these TEM images.

Table 2
Mechanical properties and toughness of neat epoxy and nanocomposites cured by DDS

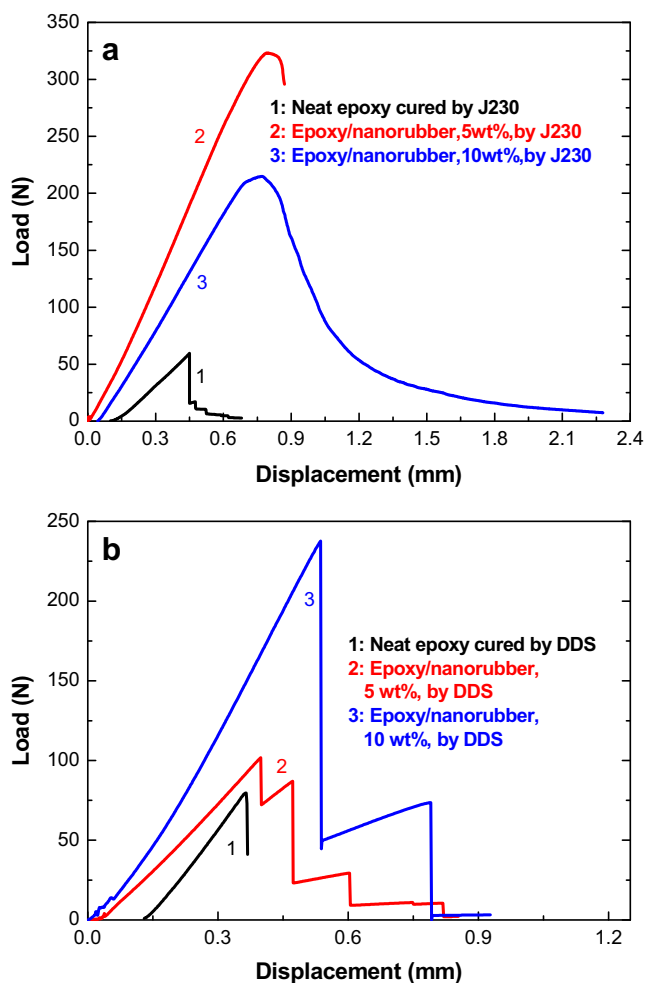| Materials	Young's modulus, GPa	Tensile strength, MPa	Plane-strain fracture toughness, K_{1c}, MPa m$^{1/2}$	Critical strain energy release rate, G_{1c}, kJ/m^2
Neat epoxy, cured by DDS	3.20 ± 0.04	88.2 ± 14.8	0.51 ± 0.04	0.073 ± 0.010
Nanocomposite, 5 wt%, cured by DDS	3.25 ± 0.20	94.7 ± 4.3	1.13 ± 0.03	0.349 ± 0.014
Nanocomposite, 10 wt%, cured by DDS	3.09 ± 0.16	90.0 ± 1.3	1.46 ± 0.059	0.696 ± 0.054

Fig. 4. The load–displacement curves of neat epoxy and nanocomposites cured (a) by J230 and (b) by DDS.

3.2. Mechanical properties and toughness

J230 and DDS were used as two hardeners to investigate the effect of matrix modulus on the mechanical properties and fracture toughness of nanocomposites. In Fig. 2, J230 is a polyether amine
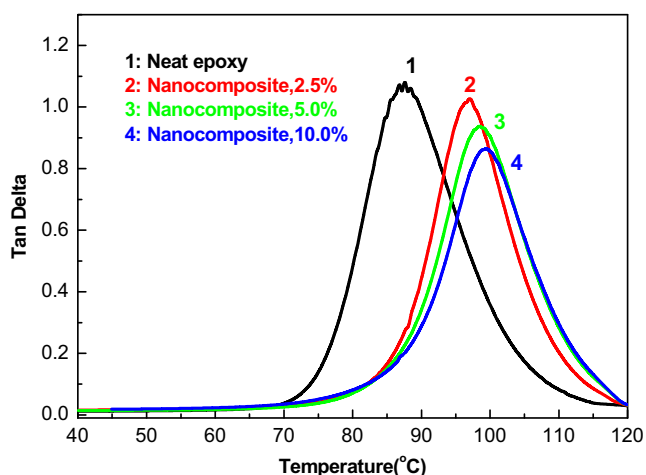

Fig. 5. DMA curves of epoxy and its nanocomposites cured by J230.

composed of 2–3 propylene oxide groups which provide relatively flexible crosslinking network, leading to a relatively ductile material's behaviour; the DDS backbone contains benzene and sulfone groups which provide the network with rigidity, leading to a brittle material's behaviour. The tensile stress–strain curves of the two hardener-cured systems are shown in Fig. 3. In both systems, elongation at break increases with the nanoparticle content, leading to an increase of the area under the curves which means the improvement of ductility. With 10 wt% nanoparticle, the J230-cured system in Fig. 2a displays higher elongation at break than the DDS-cured system in Fig. 2b, which is caused by the hardeners used.

It is noteworthy that at 10 wt%, the J230-cured epoxy indicates an obvious reduction of tensile strength while the DDS-cured epoxy shows no reduction. This is explained in the light of matrix ductility. As J230 provides epoxy with a relatively flexible crosslinking network, its tensile samples yielded before fracture. When yielding occurs, the crosslinked molecules align themselves in the tensile direction, causing a large-scale plastic deformation. Due to the large deformation, the dispersion phase—rubber nanoparticles—reasonably carries a substantial amount of load, depending on the particle fraction. Since the rubber strength is less than one third of the matrix strength [29], 10 wt% nanoparticles cause an obvious reduction. As the volume occupied by 5 wt% nanoparticles may not be sufficient to carry as a substantial load as the 10 wt% does when yielding occurs, it shows no negative effect on the tensile strength. Because DDS provides the cured epoxy with a rigid crosslinking network, its tensile samples did not yield prior to fracturing in Fig. 3b. This means that no large-scale deformation occurs when the samples fracture. In such a brittle matrix, a larger volume of nanoparticles is needed to increase the ductility of the matrix. With increase in the volume fraction, increasingly higher load is shared by the nanoparticles and this makes the matrix ductile to absorb fracture energy. The highest fraction in the DDS-cured system is 10 wt% at which no strength reduction observed, but we predict that an obvious reduction will occur if the nanoparticle fraction is further increased.

Tables 1 and 2 show the effect of nanoparticles' content on the Young's modulus, tensile strength and fracture toughness of the two systems. Regarding the J230-cured nanocomposites, no reduction of Young's modulus is visible except the 10 wt% specimen. Although the 10 wt% rubber nanoparticles reduce the tensile strength of the J230-cured epoxy 8.6%, it shows no negative effect on the DDS-cured epoxy, which confirms the observation in Fig. 3b.

It is worth to note the difference in standard deviations for the tensile strength between neat epoxy and DDS-cured nano-composites in Table 2. The large deviation of neat epoxy is caused by impurities or flaws introduced during processing, a well-known fact for brittle resin. The deviation is obviously reduced by the nanoparticles, implying that rubber nanoparticles relieve the effect of flaws on the mechanical performance, in agreement with our previous research [14] where silica nanoparticles reduced the standard deviation of tensile strength of the DDS-cured epoxy.

Both K_{1c} and G_{1c} increased significantly with the nanoparticle content in Tables 1 and 2. Merely 5 wt% rubber nanoparticles enhanced the energy release rate of the J230-cured epoxy from 0.175 to 1.710 kJ/m^2, 877% improvement, while for the DDS-cured epoxy, significant toughness improvement (853%) was obtained with 10 wt% nanoparticles. Since the DDS-cured epoxy has a higher stiffness than the J230-cured epoxy, the comparison of toughness means that a high loading of nanoparticles is indispensible to toughen high-stiffness resins. Regarding the toughness improvement, 5 wt% nanoparticles are ideal for the J230-cured system while 10 wt% for the DDS-cured system. It is noteworthy that the significantly improved fracture toughness was achieved without sacrificing other properties such as Young's modulus and tensile
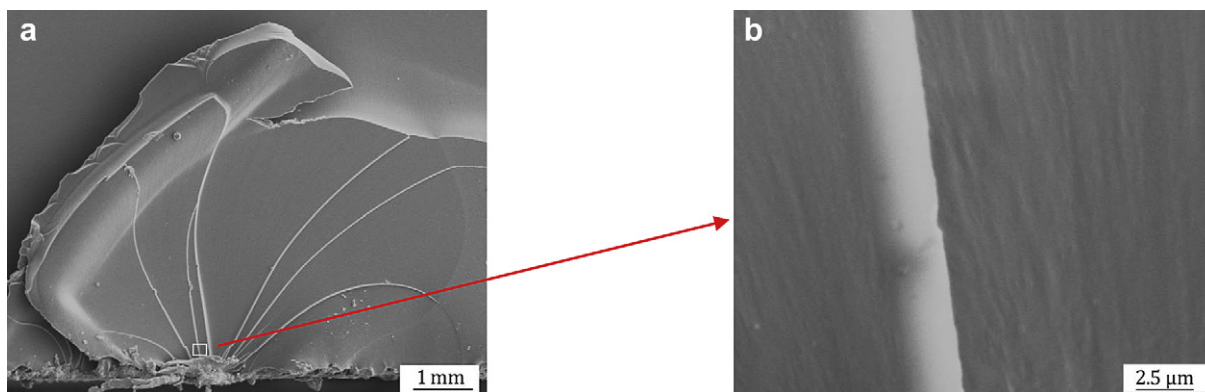
Fig. 6. SEM micrograph of tensile-fractured surface of neat epoxy cured by J230 (b is the magnified image of the tiny square in a).

strength, which may surpass all the reported values of toughness in the field of epoxy toughened by nanomaterials given similar matrix brittleness [14,23,24].

Fig. 4 shows the load vs displacement graphs of compact tension (CT) testing under a continuous loading condition with similar crack length and sample thickness for each system. The crack propagation in the J230-cured neat epoxy is unstable and exhibits a sawtooth-shaped curve, characteristic of the stick-slip mode of crack propagation. Compounding with rubber nanoparticles made the crack propagation stable, as the load graph showed yielding when the crack started propagating. This means that the nanoparticles promoted and involved in a large-scale plastic deformation. The 10 wt% sample in Fig. 4a shows a lower fracture load than the 5 wt% sample, indicating that the 10 wt% nanoparticles soften the matrix and may not toughen epoxy as significantly as the 5 wt% which is confirmed in Table 1. Regarding the DDS-cured system in Fig. 4b, the crack propagation graphs for all samples exhibit a sawtooth-shaped behaviour, meaning unstable crack propagation. But the samples show higher fracture load with increase in the nanoparticle content, corresponding to the highly improved fracture toughness as in Table 2. This implies that these two systems must have different toughening mechanisms which will be discussed in Section 3.6.

3.3. Thermal dynamic mechanical analysis

The relaxation dynamics of crosslinked epoxy molecules are highly sensitive to the local environment near its glass transition temperature (T_g). When it is heated or cooled through T_g, the properties of epoxy, such as stress–strain relation, specific volume and enthalpy, experience a dramatic change due to the rearrangement of crosslinked molecules. The rate of the rearrangement or relaxation process depends on the local environment, such as the addition of reinforcement particles and their interface. Thus, the measurement of these properties identifies the roles of nanoparticles in the thermal mechanical environment of crosslinked epoxy molecules near T_g.

Fig. 5 shows the damping behaviour of epoxy and its 2.5 wt%, 5 wt% and 10 wt% nanocomposites cured by J230. Determined from the midpoints of the corresponding glass transition regions, the T_gs for these specimens are 87.3 °C, 96.8 °C, 98.6 °C and 99.4 °C, respectively. In general three factors contribute to the change of T_g: the addition of second phase; crosslink density and the interface between matrix and dispersion phase. The addition of particles, especially nanoparticles due to their substantially higher specific surface area in comparison with micron-sized particles (denoted microparticles) which will be quantitatively compared and discussed in Section 3.5, poses barriers to the vibration of matrix molecules through the T_g region and thus causes longer relaxation time, implying higher T_gs, in agreement with previous research where silica nanoparticles increased the T_g of neat epoxy [14,30]. Crosslink density remained constant by carefully controlling the ratio of hardener to the matrix. The interface between matrix and dispersion nanoparticles in this study should be strong, otherwise the agglomeration of particles caused during curing should be observed. The strong interface enhanced the restriction effect of nanoparticle on the rate of relaxation, leading to higher T_gs.

The height and breadth of the peaks in Fig. 5 provide additional information about the relaxation behaviour of the nanocomposites. Corresponding to the increased T_gs, the reduced magnitudes of tan δ graphs are 1.09, 1.03, 0.94 and 0.87 for the neat epoxy, 2.5 wt%,
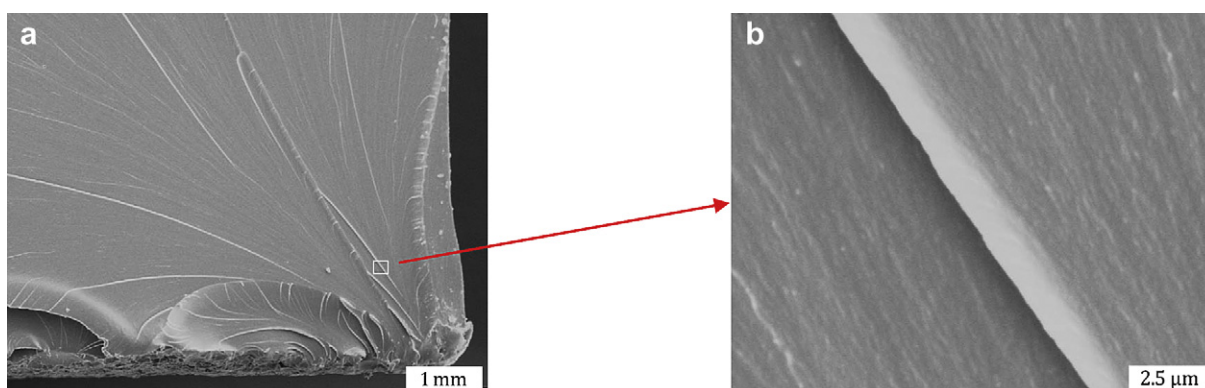

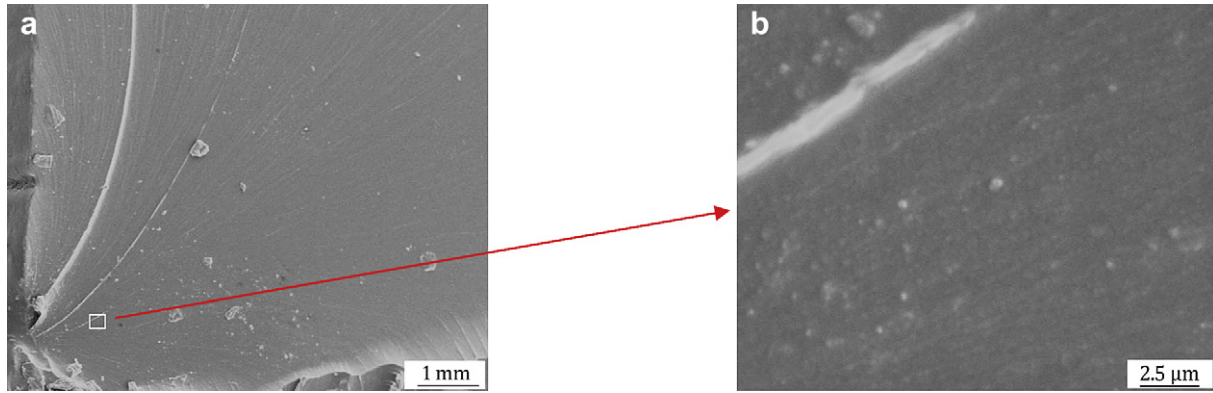**Fig. 7.** SEM micrograph of tensile-fractured surface of the 5 wt% J230-cured nanocomposite.

Fig. 8. SEM micrograph of tensile-fractured surface of the 10 wt% J230-cured nanocomposite.

5 wt% and 10 wt% systems, respectively. The magnitude reduction is caused by the increased ratio of second phase in the matrix. All the specimens show similar peak width at half height. The peak width at half height may be an indicator of the size distribution and the dispersion of particles. The peak width should increase when the dispersion particles have a large size distribution or agglomeration appears, because different particles' or agglomerations' sizes produce different restriction effects on the relaxation time of crosslinked molecules. Nanotube and nanoclay have large size distribution and once compounded with epoxy, the peak width at half height of epoxy was obviously increased [31,32]; similar effect was observed for rubber/starch composites where a large particle size distribution was found [33]. In this study, the size distribution of nanoparticles is small as shown in Fig. 1 and thus the peak width at half height of the nanocomposites is similar to that of neat epoxy, which aligns with our previous research [14].

Similar trend was found for the DDS-cured system which thus not shown.

3.4. Microcopy analysis of fracture surface

3.4.1. Tensile-fractured surface analysis

The tensile-fractured surfaces of neat epoxy and its nanocomposites cured by J230 were examined by SEM. Fig. 6 contains representative images of neat epoxy. A number of river lines are found in Fig. 6a, and rather flat surface is observed in Fig. 6b which is the magnified image of the tiny square in Fig. 6a. With 5 wt% rubber nanoparticles, more and finer river lines are observed in Fig. 7a; many fine ridges are found at a high magnification in Fig. 7b due to the presence of nanoparticles. This means that the rubber nanoparticles promote the ductile deformation of the matrix,

corresponding to the presence of yielding at break and the enhancement of elongation in Fig. 3a. Fig. 8a shows the fracture surface of the sample containing 10 wt% rubber nanoparticles, indicating less amount of river lines than the 5 wt% sample in Fig. 7a although a higher magnification in Fig. 8b demonstrates a similar degree of fine ridges to Fig. 7b. This implies that 5 wt% nanoparticles are more efficient in terms of promoting ductile fracture than 10 wt% nanoparticles which may just soften the matrix. The conclusion aligns with the reduced yield strength of the 10 wt% sample in Fig. 3a and in Table 1.

Figs. 9–11 contain the typical SEM micrographs of tensile-fractured surfaces of neat epoxy and its nanocomposites cured by DDS. The well-known 'mirror', 'mist' and 'hackle' zones [34] are clearly identified in these figures using capital letters A, B and C, although these zones are not clear on the tensile-fractured surface of the J230-cured system in Figs. 6–8 due to the ductility of the matrix. Fracture initiated from a minute flaw and grew slowly, producing a smooth fracture surface – the 'mirror' zone denoted by 'A' in Fig. 9a. This zone is circled by the 'mist' zone denoted by 'B', which is less smooth. The 'mist' zone developed into a rough surface named 'hackle' zone by the rapid propagation of the fracture in a direction perpendicular to the tensile direction. A number of dimples are observed in the 'hackle' zone, one of which is magnified in Fig. 9b. This represents the brittle failure of high modulus, homogenous materials.

With 5 wt% nanoparticles, the 'mirror' zone appears whitened in Fig. 10a and dimples are replaced by many ridges in the 'hackle' zone (Fig. 10b), indicating that the nanoparticles promoted the ductile deformation of matrix. The addition of 10 wt% rubber nanoparticles completely changed the fracture surface. The diameter of the whitened 'mirror' zone increases from ∼1 mm in Fig. 10a to ∼8 mm in Fig. 11a. At a high magnification in Fig. 11b,
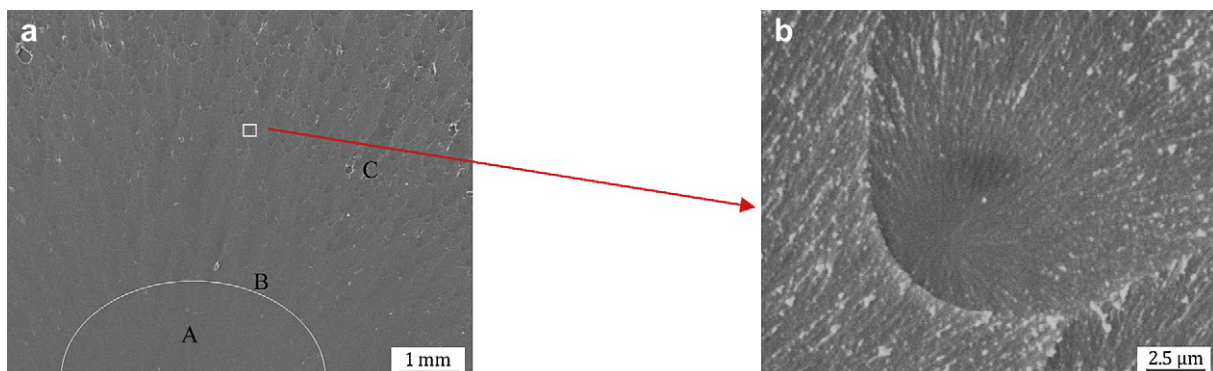

Fig. 9. SEM micrograph of tensile-fractured surface of neat epoxy cured by DDS.
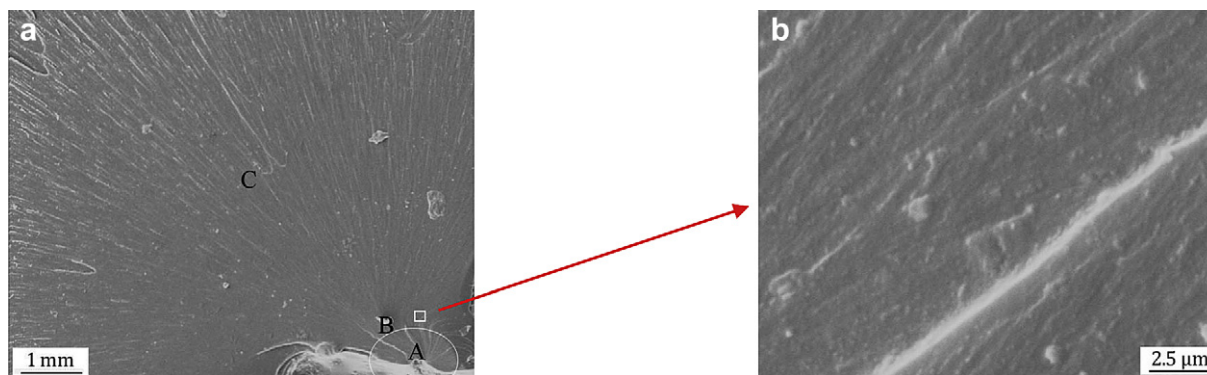
Fig. 10. SEM micrograph of tensile-fractured surface of the 5 wt% DDS-cured nanocomposite.

fibrils of 100–200 nm in diameter and 3–5 µm in length are observed. The formation of fibrils implies that the 10 wt% nano-particles caused more matrix deformation than the 5 wt%.

As the fibrils have never been reported in the literature of epoxy/rubber composites, we are curious to learn what composes the fibrils and how they are formed. Rubber nanoparticles are extremely ductile compared to brittle epoxy. Given that the large dimensional difference between the nanoparticles and the fibrils, a number of uniformly dispersed nanoparticles may deform with matrix to create fibrils under tensile loading. This explanation is supported by a previous research [26], in which nylon was used to reinforce ethylene–propylene diene monomer rubber (EPDM) with the aid of a compatilizer chlorinated polyethylene. Under tensile loading, the fibrils were formed and observed on the fracture surface (see Fig. 4 in Ref. [26]). In conclusion, spherical polymeric particles in polymer matrix are able to form fibers or fibrils under tensile loading.

3.4.2. Fracture surface analysis of compact tension (CT)

In Fig. 12, the fracture surface of the J230-cured neat epoxy is featureless and smooth, corresponding to brittle failure. Upon addition of 5 wt% rubber nanoparticles, fracture toughness increased 213.7% in Table 1 and this should be accompanied with a rough fracture surface, which is confirmed by a stress-whitened zone of ~4 mm in length on the fractured surface in Fig. 13a. Stress-whitening is due to the scattering of visible light from a layer of scattering centers, in this study voids as identified in the following TEM analysis. In comparison with Fig. 12a, the zone in Fig. 13b shows an obviously rougher, scale-like surface with large number of hackles and ridges. At a high magnification in Fig. 13c, a rough surface was observed in contrast to Fig. 12b. The highly improved surface roughness means that the matrix deformation such as shear

banding is the major fracture surface phenomenon which absorbs fracture energy. This conclusion is supported by the large-scale plastic deformation deduced in Fig. 4a. It is noteworthy that the length of stress-whitened zone extends from 4 mm for 5 wt% nanocomposite to 6 mm for 10 wt% nanocomposite, although the 10 wt% nanocomposite shows a lower toughness improvement in Table 1. This is contradictory to a known fact that the fracture toughness values of toughened epoxy increase with the size of stress-whitened zone, implying that rubber nanoparticles must work on different toughening mechanisms to their peer micro-particles. Although similar fracture features are seen in both Figs. 13c and 14c, comparison of Fig. 14b with Fig. 13b leads to a conclusion that a lower degree of ridges prevails throughout the fracture surface of the 10 wt% sample, implying that the 10 wt% particles are unable to produce a highly rough fracture surface to consume energy, as confirmed by the reduced toughness in Table 1. Actually the 10 wt% particles just soften the matrix, as supported by the reduced yield strength in Fig. 3a.

Not shown here is the fracture surface of CT of the DDS-cured neat epoxy, which is similarly smooth and mirror-like as the J230-cured epoxy in Fig. 12. Upon compounding with 5 wt% rubber nanoparticles, many ridges appear as shown in Fig. 15. Under the same magnification in Fig. 15c and Fig. 13b, the 5 wt% DDS-cured sample shows a lower degree of deformation than the 5 wt% J230-cured sample, implying the rubber nanoparticles are more efficient to promote plastic fracture deformation in a lower-stiffness matrix which leads to a high toughening effect as supported in Tables 1 and 2. With 10 wt% particles, a stress-whitened zone is observed in Fig. 16a. A little more quantity of ridges can be seen in Fig. 16b and c than in Fig. 15b and c, implying that more nanoparticles promoted more matrix deformation but not as much as that in the
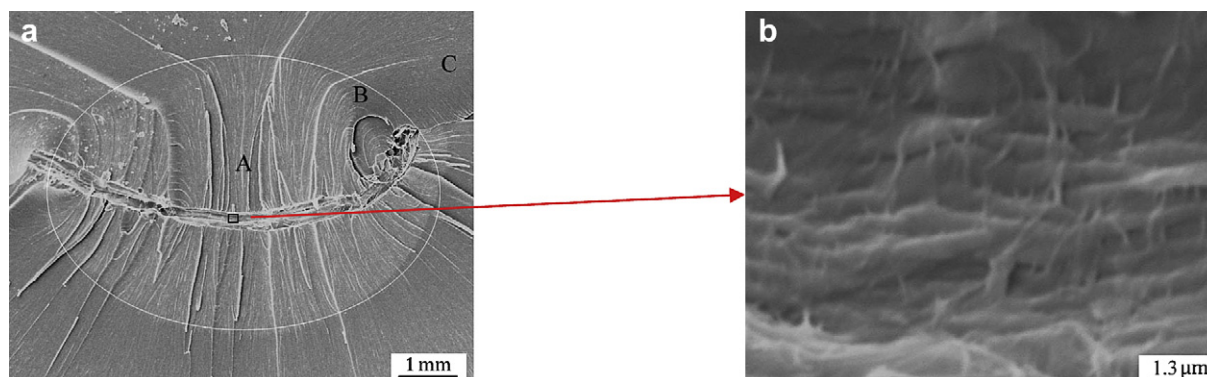

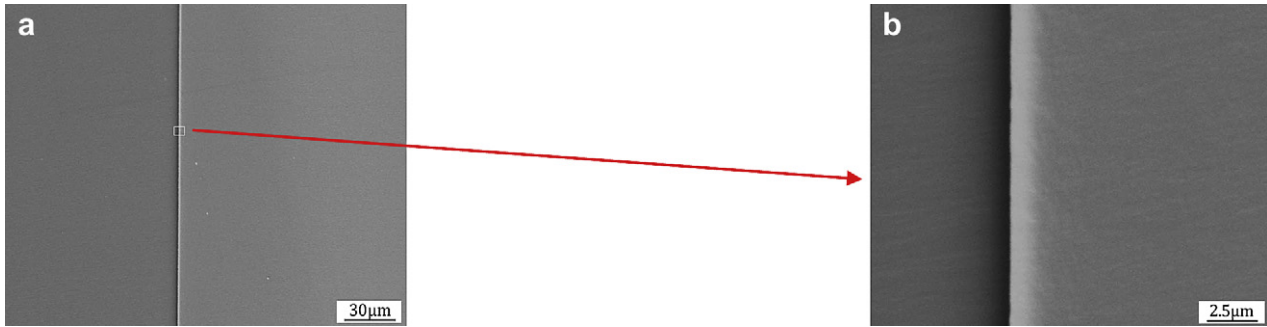**Fig. 11.** SEM micrograph of tensile-fractured surface of the 10 wt% DDS-cured nanocomposite.

Fig. 12. SEM micrograph of surface of fractured CT of neat epoxy cured by J230 (Crack propagates from left to right).

J230-cured system. This means that more rubber nanoparticles are needed to toughen a high-stiffness resin. In Fig. 16c, voids can be distinguished through careful observation. Under a higher magnification in Fig. 16d, these voids show a diameter of 73.5 ± 15.5 nm through image analysis, whose formation process will be identified in the following TEM observation and discussion.

3.5. Calculation and comparison of interparticle distance and particle surface area

Rubber nanoparticles achieved significantly toughening effect at 5 wt% in comparison with conventional epoxy/rubber composites where 15–20 wt% microparticles are indispensible for effective toughening [1,35]. It must be the particle size that makes such a great difference. Therefore, we calculated the surface–surface interparticle distance and total particle surface area for nanocomposites and composites, which were further compared and plotted.

The number of particles in a given volume V is

$$\frac{V \times a}{\frac{4}{3}\pi \times r^3}$$

where α is the volume fraction of particles, which is assumed as weight fractions as both particles and matrix are polymers, r is the radius of particle.

Assuming the same number of identical cubes which exactly fill up the volume V, the lateral size of the cubes is

$$\sqrt[3]{V \div \frac{V \times a}{\frac{4}{3}\pi \times r^3}} = r \times \sqrt[3]{\frac{4}{3a}\pi}$$

The surface–surface interparticle distance of nanoparticles is the difference between the lateral size of the cube and the diameter of the particle:

$$r * \sqrt[3]{\frac{4\pi}{3a}} - 2r = r * \left(\sqrt[3]{\frac{4\pi}{3a}} - 2 \right)$$

The total particle surface area in the volume V:

$$4\pi \times r^2 \times \frac{V \times a}{\frac{4}{3}\pi \times r^3} = \frac{3a}{r}V$$

All the particles in composites are assumed to have an identical diameter of 1 μm, and similarly all the nanoparticles in this study are treated as identical particles of 55 nm in diameter. The calculated surface–surface distance and the total particle surface area of these two systems are shown in Table 3 and are further plotted in Fig. 17a and b. While the surface–surface interparticle distance in composites obviously reduces with fraction, the interparticle distances in nanocomposites are substantially lower. With such a low interparticle distance, nanoparticles at a very low fraction interact each other much more efficiently to initiate matrix toughening mechanisms such as shear banding than microparticles. In Fig. 17b, the total particle surface area of nanoparticles increases significantly with volume fraction compared to those in composites, implying that nanoparticles are able to interact with matrix much more efficiently to promote matrix deformation. As a result, nanocomposites show a much higher toughening effect at a low particle fraction than composites in Fig. 17c.

3.6. Fracture mechanism identification

Fig. 18 contains the optical micrographs of the thin section taken from a fractured CT specimen of the 5 wt% J230-cured nanocomposite. In Fig. 18b, a birefringence zone of ~25 μm in thickness was found below the fracture surface when observed between polarizers, implying a low level of plastic deformation in the vicinity of the crack tip. By contrast, a much larger birefringent damage zone ranging from 100 to 150 μm in thickness was reported in conventional epoxy composites containing 15–20 wt% liquid rubber [see Figs. 29 and 30 in Ref. [36]], which was caused by matrix shear yielding. The comparison of the birefringence zone thickness shows that the matrix in this study experienced a much lower degree of plastic deformation, although higher fracture toughness obtained herein, contradicting to a well-known fact that a larger birefringent zone often corresponds to a higher fracture toughness. In the conventional composites, 20 wt% rubber substantially softens matrix, leading to 15–20% reduced modulus and strength, while
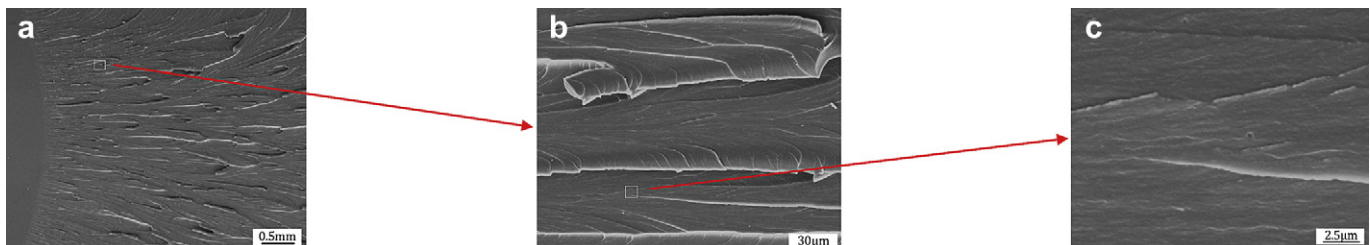

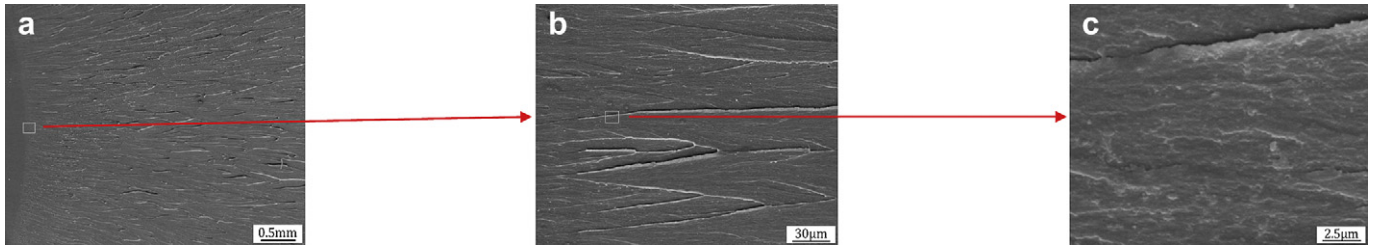**Fig. 13.** SEM micrograph of surface of fractured CT of the 5 wt% J230-cured nanocomposite.

Fig. 14. SEM micrograph of surface of fractured CT of the 10 wt% J230-cured nanocomposite.
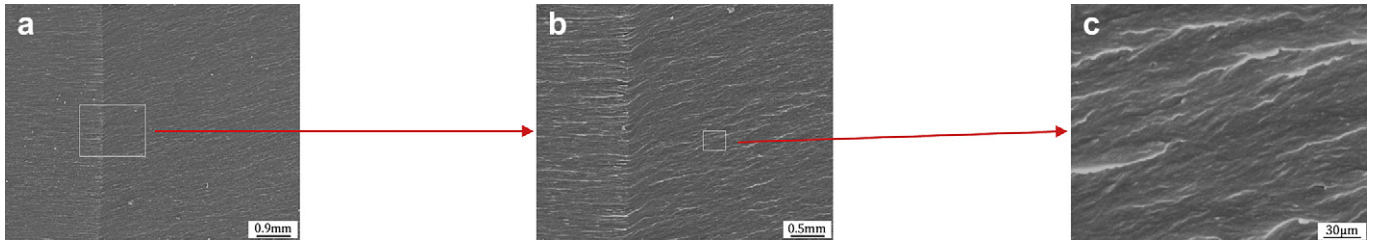

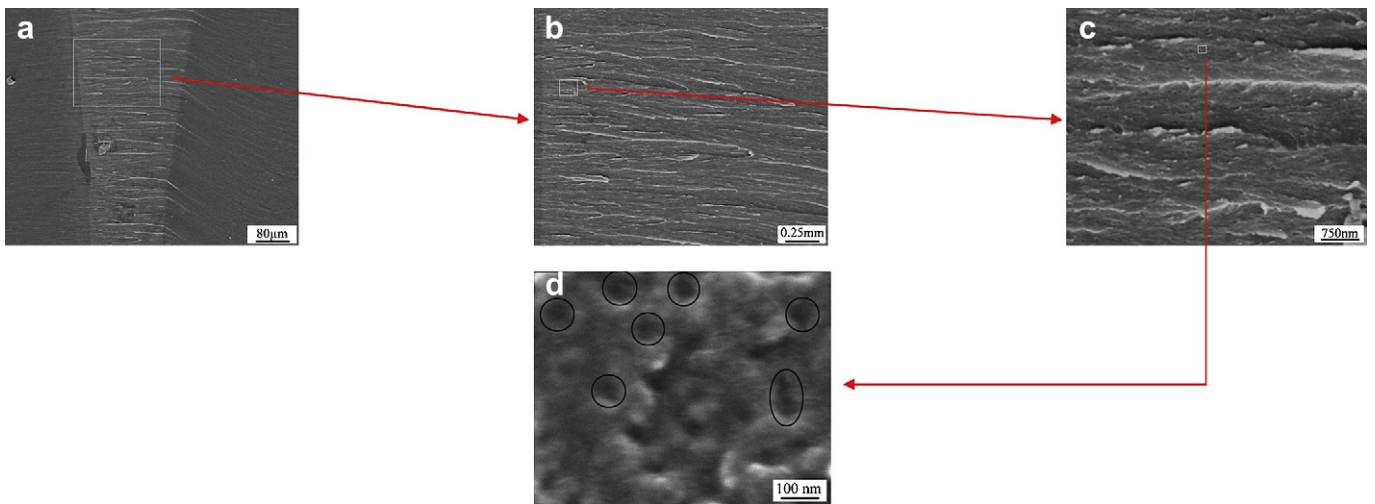**Fig. 15.** SEM micrograph of surface of fractured CT of the 5 wt% DDS-cured nanocomposite.

Fig. 16. SEM micrograph of surface of fractured CT of the 10 wt% DDS-cured nanocomposite.

there is no loss of modulus and strength in 5 wt% epoxy/rubber nanocomposite. To consume a given quantity of fracture energy, a low-modulus and -strength composite needs more plastic deformation than a high-modulus and -strength composite does. This may explain why the 5 wt% nanocomposite shows much less birefringence. In spite of the low level of birefringence, the 5 wt% rubber nanoparticles toughen epoxy superbly due to their much lower interparticle distance with substantially higher surface area than those of microparticles as shown in Fig. 17.
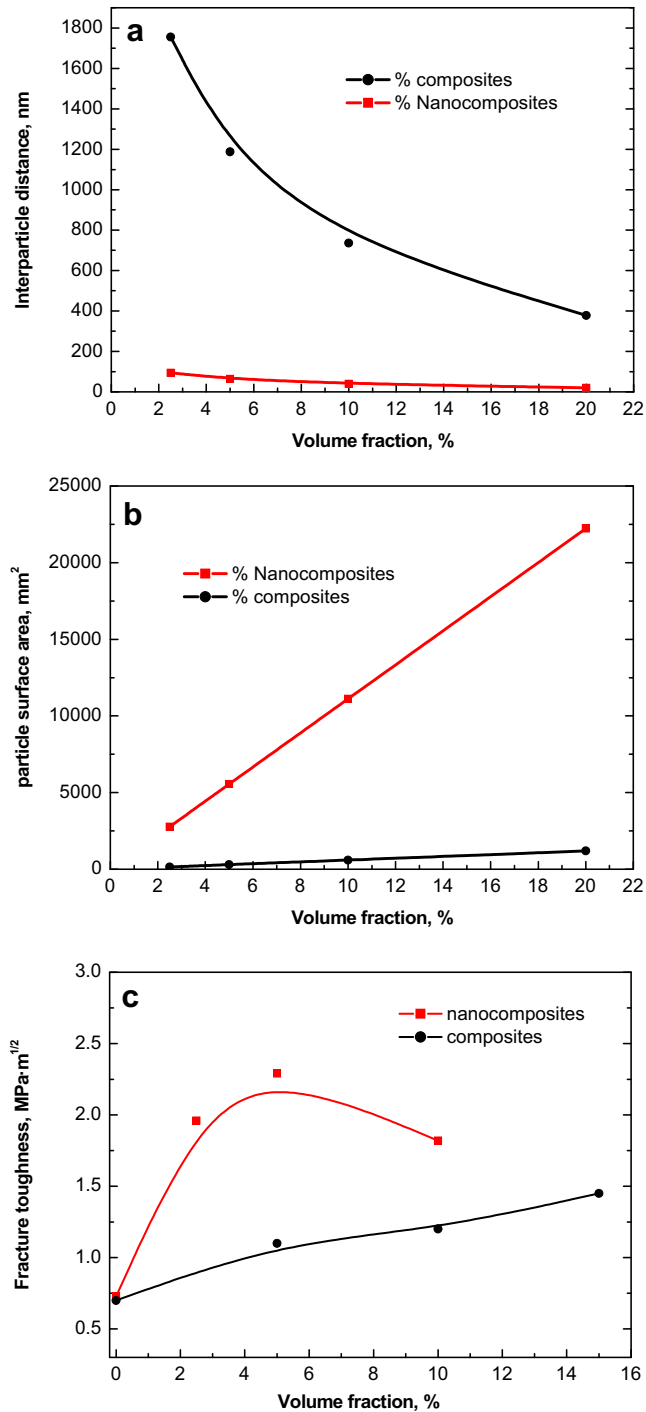
As probed in a previous work, the J230-cured neat epoxy creates a dilatation zone under a subcritical loading (see Fig 12b in Ref. [14]). Fig. 19 contains a TEM micrograph from the vicinity of a subcritical crack tip of the 5 wt% J230-cured nanocomposite without loading. While the majority of the nanoparticles appear dark due to staining, a number of nanoparticles in front of the crack are light in color due to particle dilatation. Dilatation refers to an expansion in volume of a material under stress, which appears lighter or brighter under TEM. The particle dilatation in this study was created by a tapping load applied to produce the instantly propagated crack.

Fig. 20 contains TEM micrographs from the vicinity in front of the subcritical crack tip of the 5 wt% J230-cured nanocomposite. The top image in Fig. 20 shows a 50 nm-thick section on a copper grid which includes the crack tip "A" with the following regions denoted "B" and "C". The tip is magnified in Fig. 20a where phenomena observed include (1) most rubber particles appear
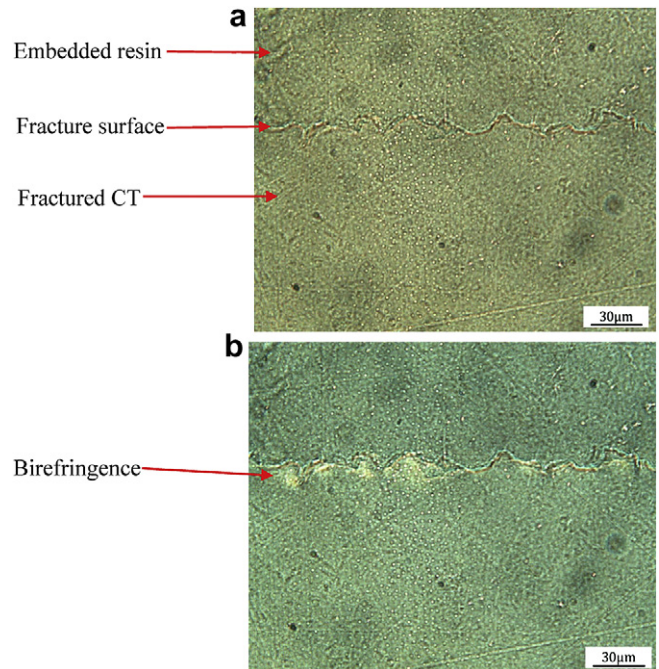
Table 3
Comparison of interparticle distance and particle surface area between composites and nanocomposites.

Particle radius, nm	Particle volume fraction	Surface–surface interparticle distance, nm	Total particle surface area in 1 mm^3, mm^2
500	0.025	1756.0	150.0
500.0	0.050	1187.4	300.0
500.0	0.100	736.2	600.0
500.0	0.200	378.0	1200.0
27.5	0.025	96.6	2727.3
27.5	0.050	65.3	5454.5
27.5	0.100	40.5	10909.1
27.5	0.200	20.8	21818.2

Fig. 18. Optical micrograph of a thin section of the embedded 5 wt% J230-cured nanocomposite perpendicular to CT fracture surface: (a) at bright field; and (b) between crossed polarizers.

in response to dilatation. The rubber nanoparticles are obviously weaker than the matrix epoxy, as rubber shows 2.2 MPa in tensile strength [37] compared with 57 MPa of neat epoxy. Due to the difference of Young's modulus and Possion ratio between epoxy and rubber, stress concentrated around rubber nanoparticles which thus dilated to grow—the void growth of matrix; this created many stress fields each of which surrounded a particle. The stress fields overlapped each other and constrained the development of the local dilatation. The expanded particles have less resistance to the penetration of electrons and thus appear whitened in Fig. 20a–c. Upon further loading, voids occurred and grew because the dilatation of particles was unable to match the deformation of the matrix. Hence, the voids grew in the loading direction with sizes larger than those of whitened particles. The matrix void growth and
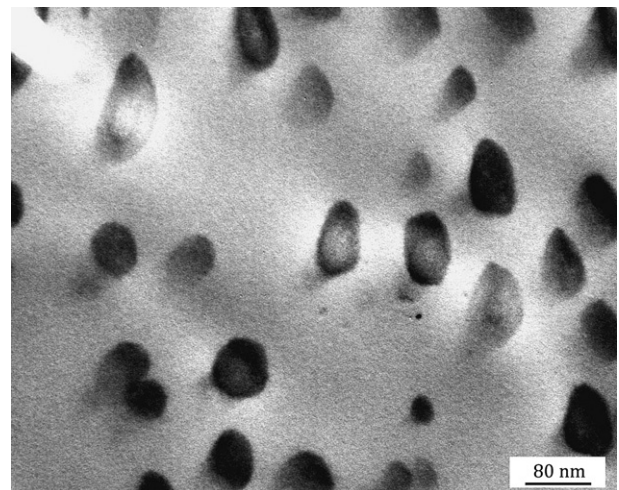

Fig. 17. Distinguishes of (a) surface–surface interparticle distance, (b) total particle surface area in 1 mm³, and (c) plane-strain fracture toughness K_{1c} of nanocomposites in this study vs conventional composites (data of composite were replotted from Fig. 3a in Ref. [1]).

Fig. 19. TEM micrographs of a propagated crack tip of the 5 wt% J230-cured nanocomposite (crack propagates from top-left to bottom-right).

whitened or developed into voids which are circled in comparison with Fig. 19 where the majority particles are black and undeformed; (2) voids deform along the loading direction perpendicular to the crack propagation trajectory; and (3) the size of the voids is larger than the whitened particles. These phenomena are explained below. Upon loading, a high stress concentration occurred at the crack tip, which caused a local dilatation. The multiphase nanostructure produced a high level of inelastic deformation
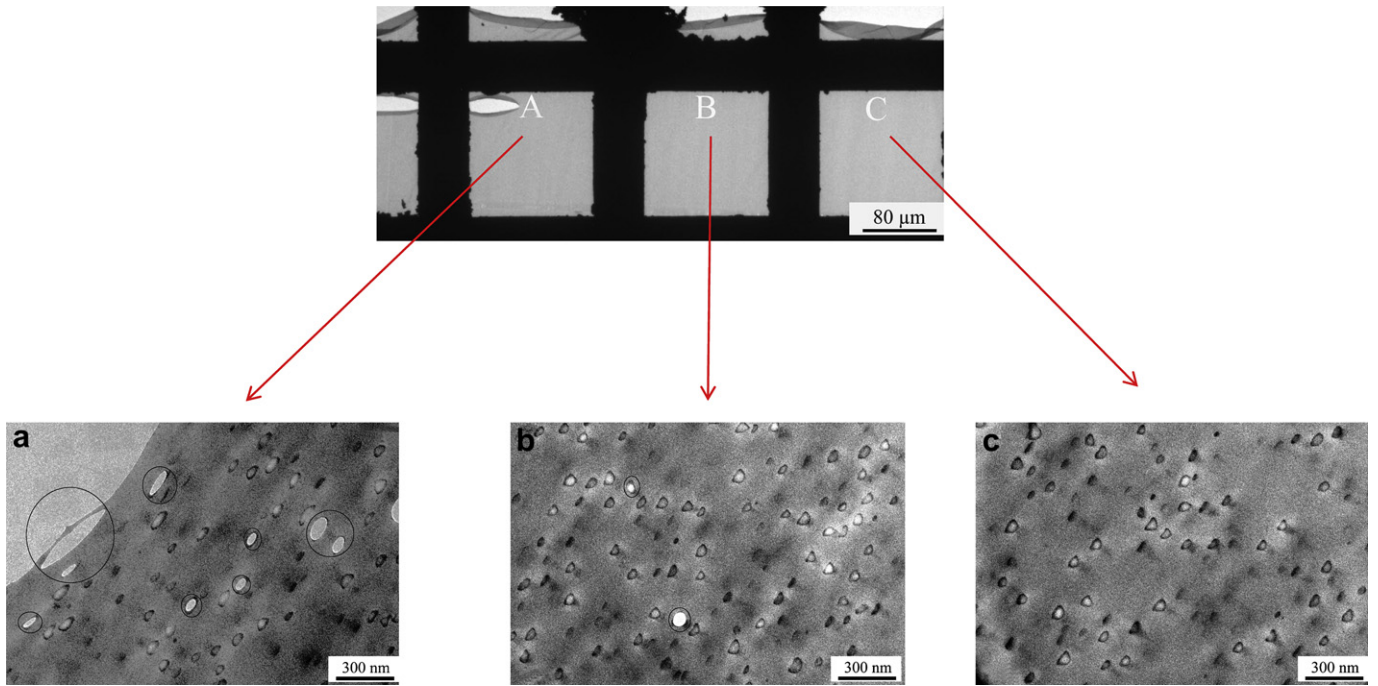
Fig. 20. TEM micrographs of a subcritical crack tip of the 5 wt% J230-cured nanocomposite: voids are circled, and other white dots represent the dilated rubber nanoparticles.
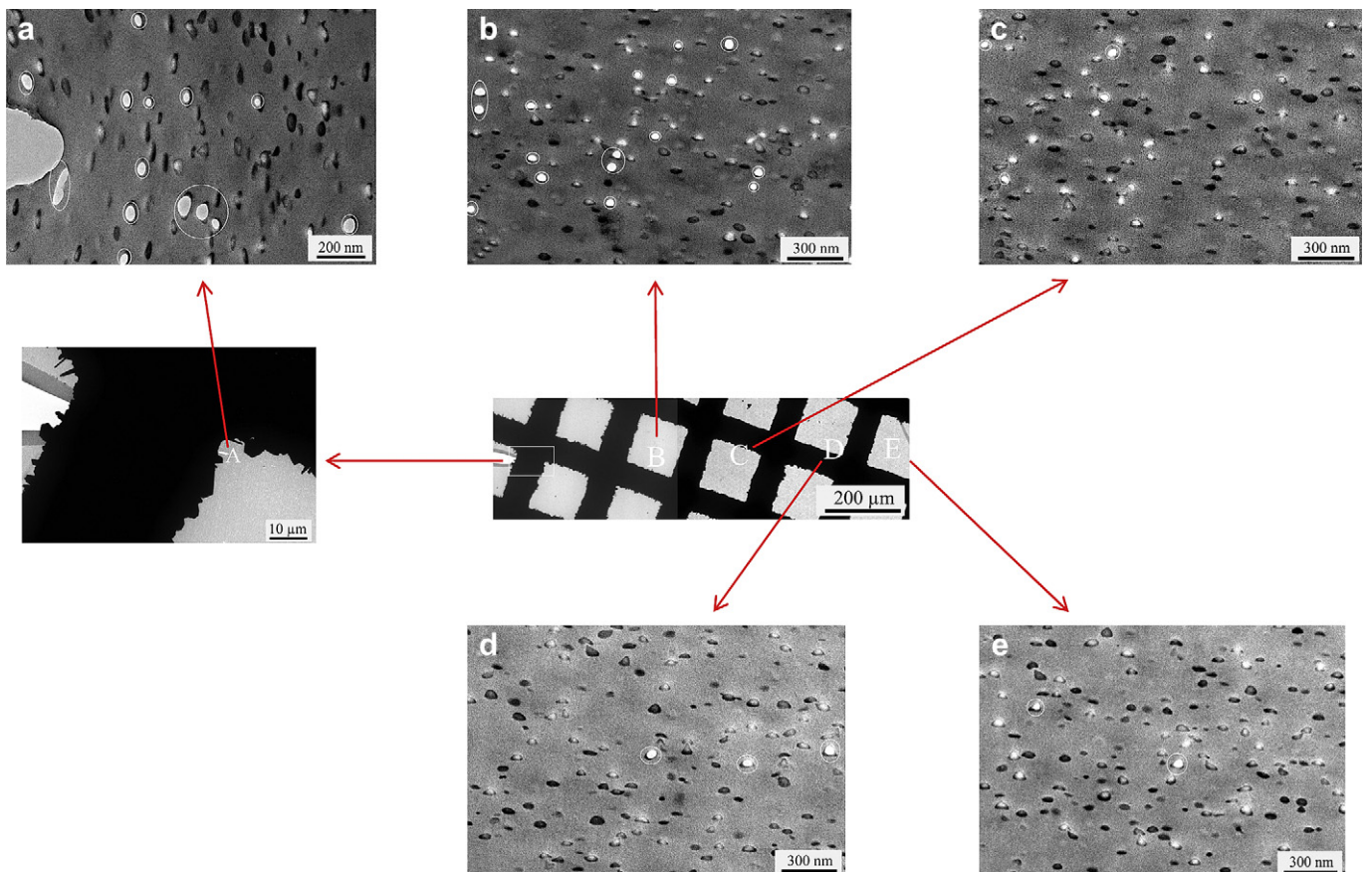

Fig. 21. TEM micrographs of a subcritical crack tip of the 10 wt% DDS-cured nanocomposite: voids are circled and other white dots represent the expanded rubber nanoparticles.

Table 4
Material properties of neat epoxy and constants used for calculation of toughness contribution.

Property	Symbol	Reference	Unit	Value
Fracture toughness of neat epoxy by DDS	K_{1c}	This work	MPa m$^{1/2}$	0.51
Tensile yield stress of neat epoxy by DDS	σ_y	This work	MPa	88.2
Compressive yield stress of neat epoxy by DDS	σ_{yc}	This work	MPa	126.0
Plane-strain compressive fracture strain of neat epoxy	γ_f	[18]		0.71
Von Mises pressure sensitivity	μ_m	[18]	–	0.2
Max stress concentration factor	K_{vm}	[19]	–	2.22

deformation initiated and promoted the matrix deformation such as shear banding, which is evidenced by the highly ridgy, scale-like fracture surface in Fig. 13 and by the birefringence in Fig. 18, leading to the highly improved toughness in Table 1.

It is worth to note that merely a portion of the particles expanded in Fig. 20a, while in conventional epoxy rubber composites, all rubber particles cavitated near the crack tip [see Figs. 4–6 of Ref. [36]]. This is explained in the light of the particle-size effect on the matrix modulus. Conventional liquid rubber-toughened epoxy contains ~20 wt% liquid rubber for effective toughening, which unfortunately reduces modulus and strength 15–20%. The softened matrix thus transfers stress more uniformly than its neat resin, causing the cavitation of all particles. In contrast, the 5 wt% rubber nanoparticles toughen epoxy significantly with no loss of modulus and strength. The high-stiffness matrix may be unable to transfer stress uniformly, causing an uneven stress distribution. As a result, only a portion of rubber nanoparticles expanded in Fig. 20a.

Fig. 20b and c shows the particle deformation further away the crack tip. A smaller amount of voids is observed, but both photos contain similar amount of whitened particles. This means the particles under loading expanded first and then voided. These whitened particles and voids caused the stress-whitened zone on the CT fracture surface as shown in Fig. 13a.

Fig. 21 contains representative micrographs of a crack tip of the 10 wt% DDS-cured nanocomposite under 50% critical loading. The photo in the centre of Fig. 21 shows a bird view, where the crack tip is squared and magnified in the left photo and further in the top-left one. In Fig. 21a, voids and whitened particles are observed. Further away the crack tip, less amount of voids is found, although the quantity of whitened particles appears similar. The voids and whitened particles explain the whitening zone in Fig. 16a. Comparing Fig. 21 with Fig. 20 leads to the following conclusion: (1) the DDS-cured nanocomposite shows more voids, which is probably caused by its higher particle content 10 wt%; and (2) the voids in the DDS-cured sample demonstrate less deformation along the tensile loading direction than the J230-cured one, which is caused by the high matrix stiffness. The DDS-cured matrix possesses a modulus 3.20 MPa compared to 2.75 MPa of the J230-cured matrix as shown in Tables 1 and 2. A higher-stiffness resin is more difficult to produce shear banding under loading, which may imply that the matrix plastic void growth plays a much more important role in the DDS-cured epoxy than the J230-cured epoxy, as confirmed by Fig. 16d.

The toughening mechanisms of 55-nm rubber particles-toughened epoxy are described as follows: (1) when subjected to loading, a high stress concentration occurs at the naturally sharp crack tip, which induces local dilatation. Stress concentrates inside these rubber nanoparticles and their surrounding region, and stress fields are formed due to the difference of Young's modulus and Possion ratio between epoxy and the nanoparticles. As a result, a portion of the nanoparticles expands. (2) With continued loading, fracture initiates inside the nanoparticles and voids are formed, as shown in Figs. 20 and 21. The formation of the voids consumes energy and relieves the geometric and stress constraint. (3) Upon further loading, the voids grow through matrix plastic deformation and finally coalescence into micro-voids and cracks, causing catastrophic fracture. In a relatively ductile matrix (J230-cured epoxy), matrix deformation such as shear banding induced by void growth is the major toughening mechanism, as supported by (i) the yielding of nanocomposites in Fig. 4a, (ii) the highly ridgy, scale-like structure in Fig. 13, (iii) the birefringence in Fig. 18, and (iv) the whitened particles and voids in Fig. 20, leading to superbly enhanced fracture toughness in Table 1. In a brittle matrix (DDS-cured epoxy) which is difficult to deform to produce shear banding, the matrix plastic void growth is most probably the major toughening mechanism, because (i) both neat epoxy and nanocomposites show unstable crack propagation in Fig. 4b, indicating the lack of large-scale matrix plastic deformation, (ii) 73.5-nm voids were found in the relatively flat, much smaller stress-whitened zone of fracture surface for the 10 wt% DDS-cured nanocomposite in Fig. 16d than that of the 5 wt% J230-cured nanocomposite in Fig. 13, and (iii) the whitened particles and voids in Fig. 21, leading to highly improved fracture toughness in Table 2.

3.7. Theoretical calculation of toughness increment for the 10 wt% DDS-cured nanocomposite

Since 73.5-nm voids were found for the DDS-cured nanocomposites in Fig. 16d, the matrix plastic void growth is most probably the major toughening mechanisms. Hence, we calculated the energy consumption using the theories and models developed by Huang and Kinloch for microparticle-toughened epoxy [38,39].

In Equation (1), a measured fracture energy G_c of the toughened resin consists of the neat resin fracture energy G_{cu} and the overall toughening contribution Ψ.

$$G_c = G_{cu} + \Psi \tag{1}$$

In this study, the overall toughening contribution comprises (i) plastic shear bands which form around the particles due to the local stress concentrations, and (ii) plastic void expansion of the epoxy matrix which develops after particle debonding. This is shown in Equation (2), where ΔG_s and ΔG_v represent the two contributions from localised shear-banding and plastic void growth of the polymer, respectively.

$$\Psi = \Delta G_s + \Delta G_v \tag{2}$$

The toughness contribution ΔG_s of plastic shear bands has been given by Huang and Kinloch as follows.

Table 5
Comparison of theoretical prediction with experimental results.

Materials	Diameter of voids	Shear banding, ΔG_f, kJ/m^2	Void growth ΔG_v, kJ/m^2	Predicted fracture energy, kJ/m^2	Measured fracture energy, kJ/m^2
10 wt% nanocomposite, cured by DDS	73.5 nm from image analysis of Fig. 16d	0.015	0.137	0.225	0.696

$$\Delta G_s = 0.5 V_f \times \sigma_{yc} \times \gamma_f \times F(r_y) \tag{3}$$

$$F(r_y) = r_y \left(\left(\frac{4\pi}{3V_f} \right)^{1/3} - \frac{54}{35} \right) \tag{4}$$

where V_f is volume fraction of dispersion particles, σ_{yc} Plane-strain compressive yield stress of the DDS-cured epoxy. It is the experimental data of tensile strength divided by 0.7 according to ASTM D5045-99 guideline, γ_f Plane-strain compressive fracture strain of the neat epoxy, r_p Radius of dispersion particles, r_y Plastic zone size of the epoxy, obtained from Ref. [40].

$$r_y = \frac{1}{6\pi} \left(\frac{K_{Ic}}{\sigma_y} \right)^2 \tag{5}$$

where K_{1c} and σ_y represent the fracture toughness and tensile yield stress of the neat epoxy, respectively.

The toughness contribution ΔG_v of plastic void growth is given in Equation (6).

$$\Delta G_v = \left(1 - \frac{\mu_m^2}{3} \right) \left(V_{fv} - V_{fp} \right) \times \sigma_{yc} \times r_y \times K_{vm}^2 \tag{6}$$

where μ_m is the yield-criteria pressure-dependency constant, K_{vm} Von Mises stress concentration, V_{fv} Volume fraction of voids caused by plastic deformation of epoxy, V_{fp} Volume fraction of dispersion particles which form void, σ_{yc}, σ_y, γ_f and r_y are the same values as in Equations (3) and (4).

These values used in the estimation of fracture energy increment are shown in Table 4.

The volume fraction of particles V_f is calculated by assuming both matrix and particles have similar densities, so that the volume fraction equals the weight fraction. Hence, for epoxy with 10 wt% rubber nanoparticles, $V_f = 0.1$. The TEM image analysis at three different locations gives a nanoparticle diameter of 55.4 ± 19.0 nm. Similarly, from the circled voids in Fig. 16d, a nanovoid diameter of 73.5 ± 15.5 nm is obtained and this gives V_v. Therefore, $(V_v − V_f)$ is known. The predicted fracture toughness contributions are compared with our experimental results in Table 5. Unfortunately, the model does not fit well the experimental data, as the contribution from ΔG_s and ΔG_v is underestimated. This means the model developed from conventional composites does not fit into nanocomposites—further work is needed to improve the model to describe the energy consumption for nanoparticles-toughened epoxy.

4. Conclusions

Using 5–10 vol% 55-nm rubber nanoparticles, the fracture toughness of the nanoparticle-modified epoxies significantly increased—K_{1c} up to 214% for the J230-cured epoxy and 186% for the DDS-cured epoxy—with no loss of strength, modulus and glass transition temperature. This superb toughness improvement at 5–10 vol% nanoparticles was explained in the light of the significantly lower surface–surface interparticle distance and the magnificently higher total particle surface area of nanoparticles dispersed in matrix than those of micron-sized particles which show merely moderate toughening effect at high loading 15–20 vol%. TEM study on subcritically propagated cracks shows that a portion of rubber nanoparticles expands, grows and deforms under loading. While the matrix shear banding is the major toughening mechanism for the J230-cured nanocomposites which show a scale-like fracture surface under SEM, the matrix void growth is the major toughening mechanism for the DDS-cured nanocomposites because 75-nm voids were found in the relatively flat, much smaller stress-whitened zone of fracture surface and both neat resin and toughened resins show unstable crack propagation.

Acknowledgments

References

[1] Xiao KQ, Ye L. Polymer Engineering and Science 2000;40:2288.
[2] LeBaron PC, Wang Z, Pinnavaia TJ. Applied Clay Science 1999;15:11.
[3] Becker O, Varley R, Simon G. Polymer 2002;43:4365.
[4] Chen JS, Poliks MD, Ober CK, Zhang YM, Wiesner U, Giannelis E. Polymer 2002;43:4895.
[5] Ratna D, Becker O, Krishnamurthy R, Simon GP, Varley RJ. Polymer 2003;44:7449.
[6] Pluart LL, Duchet J, Sautereau H. Polymer 2005;46:12267.
[7] Balakrishnan S, Start PR, Raghavan D, Hudson SD. Polymer 2005;46:11255.
[8] Boo W-J, Sun L, Warren GL, Moghbelli E, Pham H, Clearfield A, et al. Polymer 2007;48:1075.
[9] Astruc A, Joliff E, Chailan J-F, Aragon E, Petter CO, Sampaio CH. Progress in Organic Coatings 2009;65:158.
[10] Ragosta G, Abbate M, Musto P, Scarinzi G, Mascia L. Polymer 2005;46:10506.
[11] Muehlhaupt R. Adhesion; 2005:189.
[12] Sreekala MS, Eger C. Polymer composites, vol. 91. New York: Springer; 2005.
[13] Johnsen BB, Kinloch AJ, Mohammed RD, Taylor AC, Sprenger S. Polymer 2006;48:530.
[14] Ma J, Mo M, Du XS, Rosso P, Friedrich K, Kuan HC. Polymer 2008;49:3510.
[15] Chen CG, Justice RS, Schaefer DW, Baur JW. Polymer 2008;49:3805.
[16] Zhang H, Tang LC, Zhang Z, Friedrich K, Sprenger S. Polymer 2008;49:3816.
[17] Moloney AC, Kausch H, Kaiser T, Beer HR. Journal of Materials Science 1987;22:381.
[18] Lee J, Yee AF. Polymer 2001;42:589.
[19] Lee J, Yee AF. Polymer 2000;41:8363.
[20] Paul DR, Bucknall CB, editors. Polymer blends. New York: John Wiley & Sons; 2000.
[21] Sue HJ, Gam KT, Bestaoui N, Clearfield A, Miyamoto M, Miyatake N. Acta Materialia 2004;52:2239.
[22] Ma J, Mo M, Du XS, Dai SC, Luck I. Journal of Applied Polymer Science 2008;110:304.
[23] Liu J, Sue HJ, Thomson ZJ, Bates FS, Dettloff M, Jacob G, et al. Macromolecules 2008;41:7616.
[24] Liu J, Sue HJ, Thomson ZJ, Bates FS, Dettloff M, Jacob G, et al. Polymer; 2009:4683.
[25] Ma J, Qi Q, Bayley J, Du XS, Mo MS, Zhang LQ. Polymer Testing 2007;26:445.
[26] Ma J, Xu J, Zhu YJ, Zhang LQ. Polymer 2002;43:937.
[27] Kuan SC, Dai JB, Du XS, Ma J. Journal of Applied Polymer Science 2010;115:3265.
[28] Dai JB, Kuan SC, Dai SC, Ma J. Polymer International 2009;58:838.
[29] Qi Q, Wu YP, Tian M, Zhang LQ, Ma J. Polymer 2006;47:3896.
[30] Kang S, Hong S, Choe C, Kim J. Polymer 2001;42:879.
[31] Abdalla M, Dean D, Adibempe D, Nyairo E, Robinson P, Thompson G. Polymer 2007;48:5662.
[32] Wang WS, Chen HS, Wu YW, Tsai TY, Chen-Yang YW. Polymer 2008;49:4826.
[33] Tang HG, Qi Q, Wu YP, Tian M, Zhang LQ, Ma J. Macromolecular Materials and Engineering 2006;291:629.
[34] Hull D. Fractography: observing, measuring and interpreting fracture surface topography. Cambridge University Press; 1999.
[35] Thomas R, Ding Y, He Y, Yang L, Paula M, Yang W, et al. Polymer 2008;49:278.
[36] Pearson RA, Yee AFJ. Materials Science 1986;21:2475.
[37] Ma J, Xiang P, Mai YW, Zhang LQ. Macromolecular Rapid Communications 2004;25:1692.
[38] Huang Y, Kinloch AJ. Journal of Materials Science 1992;27(10):2763.
[39] Huang Y, Kinloch AJ. Journal of Materials Science 1992;27(10):2753.
[40] Atkins AG, Mai Y-W. Elastic and plastic fracture. Chichester: Ellis Horwood/ John Wiley; 1985.